

## Optimized Double ZVS-PWM Active-Clamping Forward Converter with Inputs Connected in Series and Parallel

René Torrico-Bascope<sup>(1)</sup>Fernando L. M. Antunes<sup>(1)</sup>Ivo Barbi<sup>(2)</sup>

<sup>(1)</sup>FEDERAL UNIVERSITY OF CEARÁ  
Department of Electrical Engineering  
Energy Processing and Control Group  
Fortaleza - Ceará - Brazil  
Tel.: +(55)85-288.9581 - Fax: +(55) 85-288.9574  
E-mail:rene@dee.ufc.br ; fantunes@dee.ufc.br

<sup>(2)</sup>FEDERAL UNIVERSITY OF SANTA CATARINA  
Department of Electrical Engineering  
Power Electronics Institute  
Florianópolis - Santa Catarina - Brazil  
Tel.: +(55)48-331.9204 - Fax: +(55) 48-234.5422  
E-mail: ivobarbi@inep.ufsc.br;

**Abstract** - This paper presents an isolated DC-DC converter with reduced conduction losses based on two ZVS-PWM active-clamping forward converters. In the proposed converter the inputs can be connected in series or parallel depending on the bus voltage application. To reduce rms value of the current and improve voltage and current division on the devices, the commutation inductors were coupled with adequate coupling coefficient. The converters present soft switching features from no-load to full-load condition. Theoretical analysis and experimental results taken from a 3kW laboratory prototype are presented.

### I. INTRODUCTION

Nowadays there is a demand for DC-DC topologies capable of operating with high or low bus voltage applications. To process high power, the semiconductors present technological limitation relative to voltage and/or current operation. Normally high or low bus voltage appears when three phase boost rectifiers, battery banks, solar panels and wind generators are utilized. To overcome the voltage and/or current stress, theoretically, devices in series or in parallel can be connected. On the other hand, these techniques have serious problems due to static and dynamic voltage and current division on the devices, therefore, is not recommended for practical applications. To minimize these problems multilevel cells and converters association techniques were proposed as explained in [1-6]. The converters association method is appropriate if a perfect voltage or current division between the converters can be guaranteed at any time. This condition is attainable by coupling the converters with single transformer as explained in [3-4].

The double ZVS-PWM active-clamping forward converter is based on two active clamping converters presented in [7-8]. The double converter, with uncoupled commutation inductors studied in [10-11], presents excessive reactive circulating current through the components generating high conduction losses. Therefore, to minimize this circulating current and to improve the voltage and current division across the circuits, the commutation inductors were coupled with adequate

coupling coefficient as is shown in Fig. 1. The converter maintains soft commutation features of the switches from no-load to full-load condition. To connect inputs in series, as is shown in Fig. 2.a, the input sources of the Fig. 1, are replaced by high capacitance capacitors.

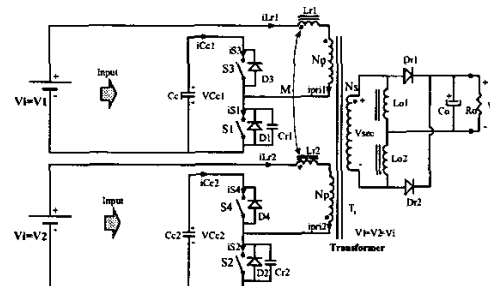


Fig. 1. Proposed converter.

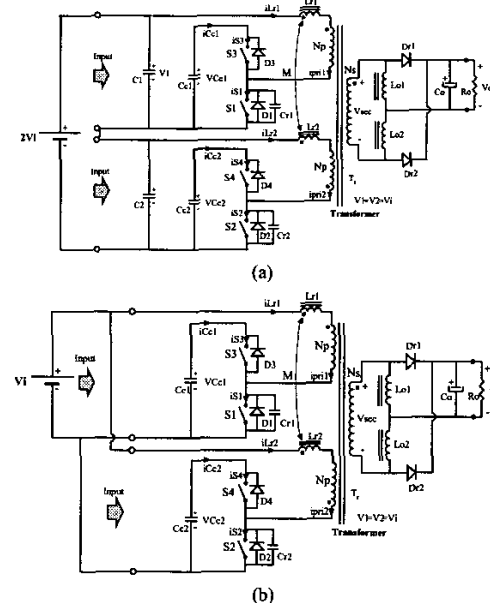


Fig. 2. Proposed converter with inputs connected; (a) in series; (b) in parallel.

## II. CIRCUIT DESCRIPTION AND PRINCIPLE OF OPERATION

### A. Circuit Description

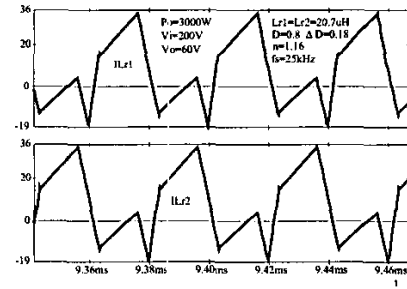
The proposed converter, shown in Fig. 1, is composed by the following components: input voltage sources  $V_1=V_2=V_i$ , input capacitors  $C_1$  and  $C_2$ , clamping capacitors  $C_{c1}$  and  $C_{c2}$ , main switches  $S_1$  and  $S_2$ , auxiliary switches  $S_3$  and  $S_4$ , coupled commutation inductors  $L_{r1}$  and  $L_{r2}$ , commutation capacitors  $C_{r1}$  and  $C_{r2}$ , antiparallel diodes  $D_1$ ,  $D_2$ ,  $D_3$ , and  $D_4$ , three-winding high-frequency transformer  $T_r$ , rectifier diodes  $D_{r1}$  and  $D_{r2}$ , output filter, consisting of  $L_{o1}$ ,  $L_{o2}$ , and  $C_o$ , and load resistor  $R_o$ .

### B. Principle of Operation

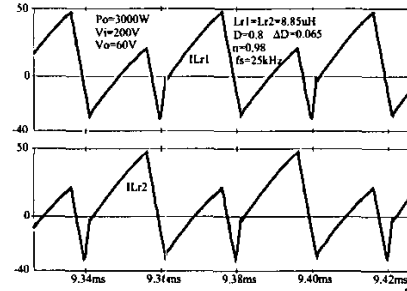
The proposed converters operate in continuous conduction mode (CCM) with soft-commutation of the controlled switches and constant frequency using asymmetrical PWM strategy shown in [9-11]. The assumed PWM strategy consists of two pulses with width smaller than  $T_s/2$  to control the switches  $S_1$ - $S_2$ , and two pulses with width bigger than  $T_s/2$  to control the switches  $S_3$ - $S_4$  as shown in Fig. 2. The indicated pulses are complementary and easily obtained using the known PWM regulator (SG3525).

To follow is explained, why commutation inductors were coupled in the proposed converter. The main objective was to reduce the excessive reactive current circulating on the converter published in [11], which presents the current waveforms shown in Fig. 3.a. To reduce such a current, the first try was to reduce inductance of the commutation inductors, on the other hand, this idea increases the rms value of the circulating current as it is shown in the waveform of Fig. 3.b. The problem was solved by coupling the commutation inductor with adequate coupling coefficient lower than one ( $K < 1$ ). If the coupling coefficient of the inductors is close to one, the reactive current to charge and discharge the commutation capacitors in parallel with switches is almost zero and as consequence the switches operate with hard commutation. The adequate coupling coefficient for the proposed converter was  $K=0.7$  and the waveforms for  $K=0.7$  are shown in Fig. 3.c. Where it is observed lower peak current when compared with the waveforms shown in Fig. 3.a and Fig. 3.b.

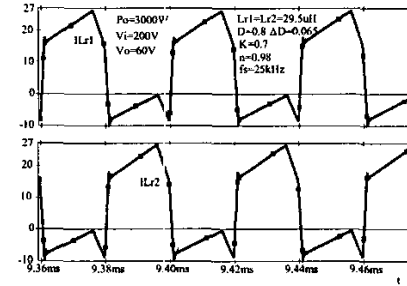
Analyzing the converter with coupled inductors, when current slopes through inductors have the same sign, the self-inductance is added to the mutual inductance ( $L_r+M$ ), and when current slopes through inductors present different sign, the resultant inductance is equal to self-inductance minus mutual inductance ( $L_r-M$ ). Thus, during power transfer and diode freewheeling interval, the resultant inductance is ( $L_r+M$ ), and during duty cycle reduction interval the resultant inductance is ( $L_r-M$ ). As both self-inductances of the commutation inductors are equal, they are named as  $L_r=L_{r1}=L_{r2}$ .



(a)



(b)



(c)

Fig. 3. (a) Uncoupled inductor currents for  $\Delta D=0.18$ ; (b) uncoupled inductor current for  $\Delta D=0.065$ ; (c) coupled inductor current for  $\Delta D=0.065$ .

## III. THEORETICAL ANALYSIS

The duty cycle ( $D$ ) and commutation period ( $T_s$ ) for the proposed converter are defined by (1) and (2)

$$D = \frac{t_w}{T_s/2} \quad (1)$$

$$T_s = \frac{1}{f_s} \quad (2)$$

In (1) and (2),  $t_w$  and  $f_s$  are the gate pulse width of switch  $S_1$  or  $S_2$  and the commutation frequency.

### A. Clamping Characteristic

The clamping voltage  $V_{Cc}$  is obtained by determining the average voltage value across the main switch  $S_1$  and applying Kirchhoff's law to the mesh formed by  $S_1$ , the transformer's upper primary,  $L_{r1}$  and  $V_i$ . Therefore,

$$V_{Cc} = \frac{2}{(2-D)} \cdot V_i \quad (3)$$

In (3),  $V_i$  is input voltage.

The graph of clamping voltage  $V_{Cc}$ , as a function of the duty cycle  $D$ , is shown in Fig. 14.

### B. Output Characteristic

In the proposed converter the duty cycle reduction  $\Delta D$  occurs due to the linear variation of the current through the coupled commutation inductors ( $L_{r1}$ ,  $L_{r2}$ ) and transformer leakage inductances. During this condition there is no power transfer from the input. The duty cycle reduction is reflected in the transformer secondary voltage.

Considering that the commutation time is much smaller than the switching period, the average output voltage and secondary voltage of the transformer, are given by (4) and (5)

$$V_o = V_{sec} \cdot \left( \frac{D}{2} - \frac{\Delta t_1}{T_s} \right) \quad (4)$$

$$V_{sec} = n \cdot \frac{V_{Cc}}{2} \quad (5)$$

In (4) and (5),  $\Delta t_1$  and  $n$  are, time interval with no power transfer, and transformer turns ratio ( $N_s/N_p$ ).

The interval  $\Delta t_1$  in a half period is

$$\Delta t_1 = \frac{n \cdot I_o \cdot L_r \cdot (2-D) \cdot (1-K^2)}{2 \cdot V_i \cdot (1+K)} \quad (6)$$

The duty cycle reduction in one period  $T_s$  is given by (7)

$$\Delta D = \frac{2 \cdot \Delta t_1}{T_s} \quad (7)$$

Substituting (6) in (7) yields

$$\Delta D = \frac{f_s \cdot L_r \cdot n \cdot I_o \cdot (2-D) \cdot (1-K^2)}{V_i \cdot (1+K)} \quad (8)$$

In (8),  $I_o$ ,  $L_r$  and  $K$  are, average output current, inductance and coupling coefficient of the commutation inductors.

Substituting (3), (5), and (6) in (4), the average output voltage obtained is given by (9)

$$V_o = n \cdot V_i \cdot \left[ \frac{D}{2 \cdot (2-D)} - \frac{f_s \cdot L_r \cdot n \cdot I_o \cdot (1-K^2)}{2 \cdot V_i \cdot (1+K)} \right] \quad (9)$$

The graph of output voltage  $V_o$  as a function of the output current  $I_o$ , known as output characteristic, is shown in Fig. 15.

### C. Commutation Analysis

The converter presents turn-on and turn-off soft switching commutations.

• *Turn on:* the normalized discharge time interval of the commutation capacitor during turn-on in non-load condition (critical situation) is given by (10)

$$\begin{aligned} \overline{t_{on}} = & \frac{\bar{f}}{2\pi} \sqrt{(1-K^2)} \left\{ \tan^{-1} \left[ \frac{-\pi \cdot (1-D)}{2 \cdot \bar{f} \sqrt{(1-K^2)}} \right] + \right. \\ & \left. + \cos^{-1} \left[ \frac{-2 \cdot \bar{f} \cdot (2-D+KD) \sqrt{(1+K)}}{D \cdot \sqrt{\pi^2 \cdot (1-D)^2 (1-K) + 4 \cdot \bar{f}^2 (1-K^2) (1-K)}} \right] \right\} \quad (10) \end{aligned}$$

$$\overline{t_{on}} = \frac{t_{on}}{T_s} \quad (11)$$

$$\bar{f} = \frac{f_s}{f_o} \quad (12)$$

$$\omega_o = 2 \cdot \pi \cdot f_o = \frac{1}{\sqrt{(L_r + M) \cdot C_r}} \quad (13)$$

Where,  $\bar{f}$  is a normalized frequency,  $f_o$  is a resonant frequency, and  $t_{on}$  is a discharge time interval of the commutation capacitor ( $C_r=C_{r1}=C_{r2}$ ).

The normalized discharge time interval  $\overline{t_{on}}$ , as a function of  $\bar{f}$ , during turn-on is shown in Fig. 4.

• *Turn-off:* the normalized charge time interval during turn-off in non-load condition (critical situation) is given by (14).

$$\begin{aligned} \overline{t_{off}} = & \frac{\bar{f}^2 (1+K)(2-D) + \bar{f} \sqrt{(1-K^2)}}{\pi^2 D (1-D)} \left\{ \tan^{-1} \left[ \frac{-\pi(1-D) \sqrt{(1-K)}}{2K \bar{f} \sqrt{(1+K)}} \right] + \right. \\ & \left. + \cos^{-1} \left[ \frac{-2D \bar{f} (1-K) \sqrt{(1+K)}}{\sqrt{\pi^2 D^2 (1-D)^2 (1-K) + 4 \bar{f}^2 K^2 D^2 (1+K)}} \right] \right\} \quad (14) \end{aligned}$$

$$\overline{t_{off}} = \frac{t_{off}}{T_s} \quad (15)$$

The normalized charge time interval  $\overline{t_{off}}$ , as a function of  $\bar{f}$ , during turn-off is shown in Fig. 5.

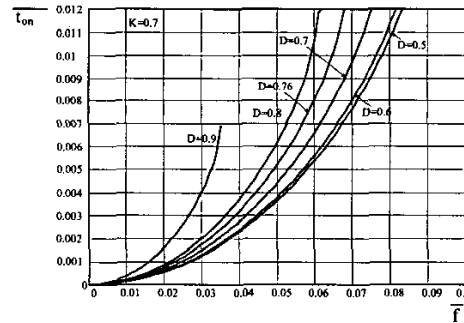


Fig. 4. Normalized discharge time interval  $\overline{t_{on}}$ , as a function of  $\bar{f}$ , during turn-on.

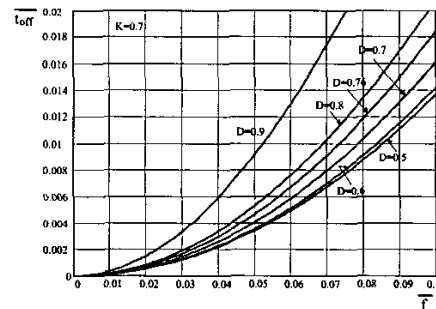


Fig. 5. Normalized charge time interval  $\overline{t_{off}}$ , as a function of  $\bar{f}$ , during turn-off.

#### D. Relevant Design Curves

In Fig. 6 the ratio between the average input current and the rms value of the commutation inductor current, as a function of the duty cycle reduction, for one forward converter, is represented. For a given duty cycle, the maximum point of the curve represents the smallest amount of reactive energy circulating in the primary side of the transformer. In practice, once a maximum duty cycle is assumed, the corresponding curve provides the reduction,  $\Delta D$ .

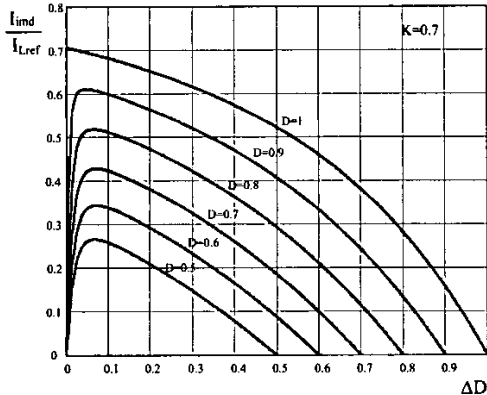


Fig. 6. Average input current and rms commutation inductor current ratio, as a function of  $\Delta D$ .

#### IV. SIMPLIFIED DESIGN EXAMPLE

A methodology and design procedure is presented in this section.

##### A. Input data

$V_i=200\text{V}$	(input voltage)
$V_o=60\text{V}$	(output voltage)
$I_o=50\text{A}$	(output current)
$P_o=3\text{kW}$	(output power)
$f_s=25\text{kHz}$	(switching frequency).

Considering ideal semiconductors, maximum duty cycle of  $D_{\max}=0.8$ , and coupling coefficient of  $K=0.7$ , the duty cycle reduction from Fig. 6 is equal to  $\Delta D_{\max}=0.065$ .

The turns ratio of the transformer is obtained from (8) and (9). Therefore,

$$n = \frac{N_S}{N_P} = \frac{2 \cdot (2 - D_{\max})}{(D_{\max} - \Delta D_{\max})} \cdot \frac{V_o}{V_i} = \frac{2 \cdot (2 - 0.8)}{(0.8 - 0.065)} \cdot \frac{60}{200} = 0.98$$

The clamping voltage is obtained from (3)

$$V_{C_c} = \frac{2}{(2 - D_{\max})} \cdot V_i = \frac{2}{(2 - 0.8)} \cdot 200 = 333.34\text{V}$$

##### B. Commutation Coupling Inductors $L_{r1}$ , $L_{r2}$

The self-inductances are determined using (8)

$$L_r = L_{r1} = L_{r2} = \frac{V_i \cdot \Delta D_{\max} \cdot (1 + K)}{f_s \cdot n \cdot I_o \cdot (2 - D_{\max}) \cdot (1 - K^2)}$$

$$L_r = L_{r1} = L_{r2} = \frac{200 \cdot 0.065 \cdot (1 + 0.7)}{25 \cdot 10^3 \cdot 0.98 \cdot 50 \cdot (2 - 0.8) \cdot (1 - 0.7^2)} = 29.5\mu\text{H}$$

When two commutation inductors of  $L_{r1}=L_{r2}=29.5\mu\text{H}$  are coupled with coupling coefficient of  $K=0.7$ , the mutual inductance is equal to

$$M = K \cdot L_{r1} = 0.7 \cdot 29.5 = 20.65\mu\text{H}$$

The leakage inductance of the coupled inductors with coupling coefficient of  $K=0.7$  is

$$L_{r1d} = L_{r1} - M = 29.5 - 20.65 = 8.85\mu\text{H}$$

The equivalent circuit is shown in Fig. 7.

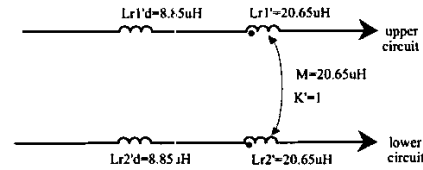


Fig. 7. Equivalent circuit of two coupled inductors with  $K=0.7$ .

##### C. Commutation Capacitor $C_r$

In the converter, turn-on is more critical of than turn-off, due to resonant commutation process.

Assuming the commutation time interval equal to 1% of period  $T_s$ , the normalized commutation time interval is obtained from (11).

$$\frac{t_{\text{on}}}{T_s} = \frac{t_{\text{on}}}{T_s} = \frac{400 \cdot 10^{-9}}{40 \cdot 10^{-6}} = 0.01$$

From the curves shown in Fig. 4 taking  $D \approx 0.76$  (obtained from (9) for  $I_o=0$ ) as parameter, the normalized frequency is  $\bar{f} = 0.065$

From (12), the resonant frequency,  $f_o$ , is

$$f_o = \frac{f_s}{\bar{f}} = \frac{25 \cdot 10^3}{0.065} = 384615.38\text{Hz}$$

Finally, using (13), the capacitance results

$$C_r = C_{r1} = C_{r2} = \frac{1}{50.15 \cdot 10^{-6} \cdot (2 \cdot \pi \cdot 384615.38)^2} = 3.4\text{nF}$$

Other design components can be obtained from reference [11].

#### IV. EXPERIMENTAL RESULTS

##### A. Results with Inputs Connected in Series

The waveforms and curves were obtained with input voltage  $2V_i=400\text{V}$  and the output voltage  $V_o=60\text{V}$ .

##### • Waveforms

The waveforms obtained for full load ( $P_o=3000\text{W}$ ) are shown in Figs. 8, 9 and 10; and for no-load ( $P_o=0\text{W}$ ) are illustrated in Figs. 11 and 12. These results confirm the soft commutation of the switches.

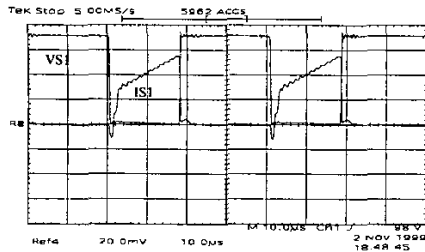


Fig. 8. Voltage and current of main switch  $S_1$  (100V/div.; 10A/div.; 10µs/div.).

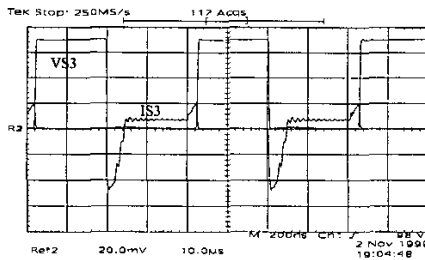


Fig. 9. Voltage and current of auxiliary switch  $S_3$  (100V/div.; 10A/div.; 10µs/div.).

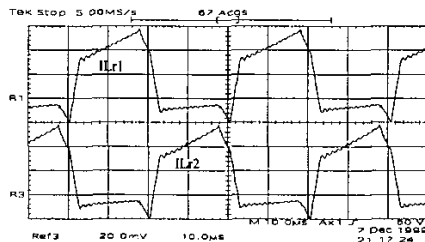


Fig. 10. Currents through inductors  $L_{r1}$  and  $L_{r2}$  (10A/div.; 10µs/div.).

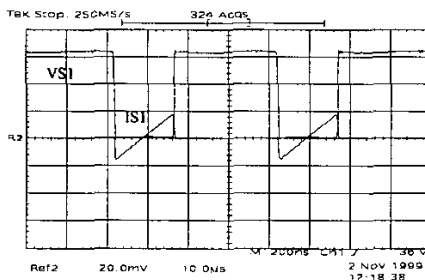


Fig. 11. Voltage and current of main switch  $S_1$  (100V/div.; 10A/div.; 10µs/div.).

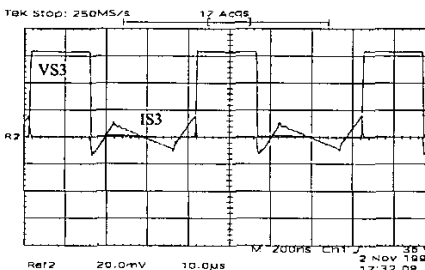


Fig. 12. Voltage and current of auxiliary switch  $S_3$  (100V/div.; 10A/div.; 10µs/div.).

• Curves

Fig. 13 shows voltage curves across input capacitors as a function of the output load current  $I_o$  connecting inputs in series, where 1.0V unbalanced that represents 0.5% of the theory value  $V_1=V_2=V_i=200V$  is observed. Figs. 14 and 15 show the clamping characteristic and the output characteristics of the converter.

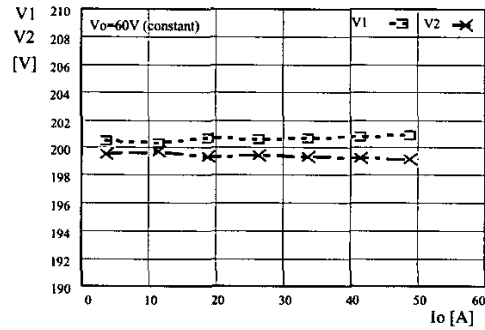


Fig. 13. Voltages across input capacitors  $C_1$  and  $C_2$ .

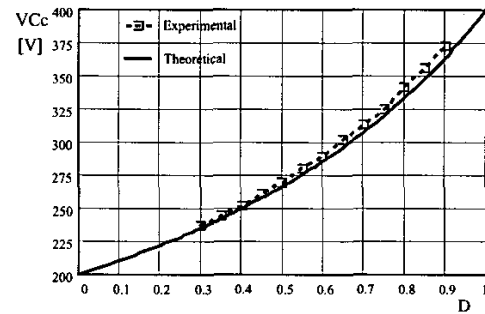


Fig. 14. Clamping characteristic of the converter.

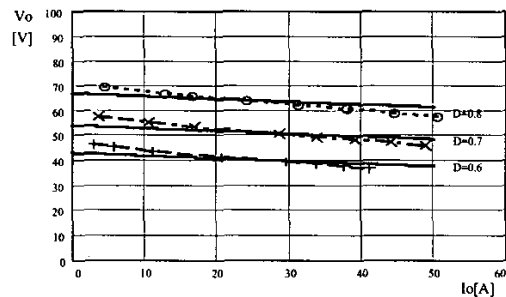


Fig. 15. Output characteristic of the converter.

B. Results with Inputs Connected in Parallel

• Waveforms

The waveforms and curves were obtained with input voltage  $V_i=200V$  and output voltage  $V_o=60V$ . In the experimental tests, the same commutation inductors in input series connection were utilized.

The voltages and currents waveforms in the switches connecting inputs in parallel are similar to the shown in the series connection section.

Fig. 16 shows commutation inductors current for full load condition.

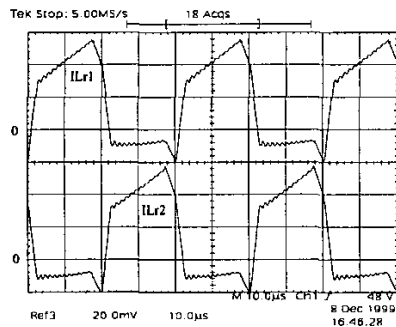


Fig. 16. Currents through inductors  $L_{r1}$  and  $L_{r2}$  (10A/div.; 10µs/div.).

• Curves

Fig. 17 shows average current curves through transformer primary windings, where current balance is observed. Therefore, the transformer does not present saturation problems.

Efficiency curves of the converter with inputs connected in series and parallel are shown in Figs. 18.

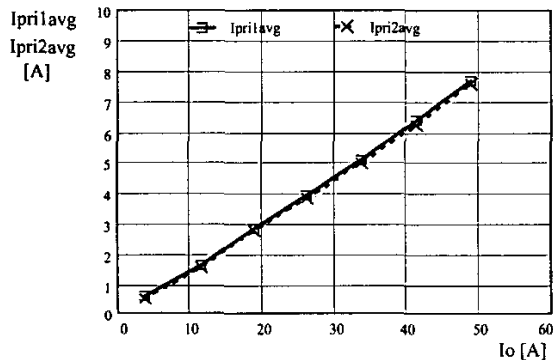


Fig. 17. average current through transformer primary windings.

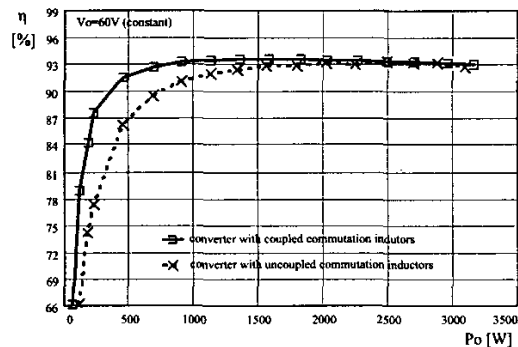


Fig. 18. Measured efficiency of the converter.

V. CONCLUSIONS

An optimized DC-DC converter capable of operating in high voltage and low voltage applications based on two single ZVS-PWM active-clamping forward converters was proposed in this paper. Analysis of the clamping characteristic, output characteristic, and experimental results taken from 3kW prototype were presented.

For the series connected inputs, the voltage unbalance across the input capacitors is 1V which corresponds to 0.5% of the theoretical value of  $V_i=200V$ . In comparison to the converter with uncoupled commutation inductors, the voltage unbalance was reduced from 5V to 1V.

Similarly, For parallel connected inputs the average current unbalance of the primary windings is negligible in comparison to the converter with uncoupled commutation inductors. The current unbalance was reduced of 0.33A to negligible value. Therefore, the transformer does not present saturation problems.

Relative to the converter with uncoupling commutation inductors, the efficiency of the converter was improved from no-load to half-load condition.

REFERENCES

- [1] T. A. Meynard, H. Foch. "Multi-level Conversion: High Voltage Choppers and Voltage-Source Inverters", in *IEEE Power Electronics Specialists Conference (PESC) Rec.*, 1992, pp. 397-403.
- [2] J. R. Pinheiro, I. Barbi. "The Three-Level ZVS-PWM DC-to-DC Converter", in *IEEE Transactions on Power Electronics*, Vol.8, No 4, October 1993, pp. 486-492
- [3] M. Miller, A. Buffin and U. Carlsson. "High Frequency ZVS for High Power Rectifiers", in *International Telecommunication Energy Conference (INTELEC) Proc.*, 1993, pp. 424-430.
- [4] M. Miller, A. Buffin and U. Carlsson. "A Versatile 48V/60V 100A Rectifiers for all Mains Inputs", in *International Telecommunication Energy Conference (INTELEC) Proc.*, 1995, pp. 466-470.
- [5] N. Kutkut, G. Luckjitt and D. Divan. "A Dual Bridge High Current DC-to-DC Converter with Soft Switching Capability", in *IEEE Industry Applications Society (IAS) Conf. Rec.*, 1997, pp. 1398-1405.
- [6] Nasser H. Kutkut. "A New Dual-Bridge Soft Switching DC-to-DC Power Converter for High Power Applications", in *Industrial Electronics Conference Records (IECON'99)*, pp. 474-479.
- [7] B. Carsten, "Design Techniques for Transformers Active Reset Circuits at High Frequencies and Power Levels", in *High Frequency Power Conversion (HFPC) conf. proc.*, 1990, pp. 235-246.
- [8] C. M. C. Duarte, and I. Barbi, "A Family of ZVS-PWM Active-Clamping DC-to-DC Converters: Synthesis, Analysis, Design, and Experimentation", in *IEEE Transactions on Circuits and Systems*, august 1997, vol.44, No. 8, pp. 698-704.
- [9] P. Imbertson and N. Mohan, "Asymmetrical Duty Cycle Permits Zero Switching Loss in PWM Circuits with No Conduction Loss Penalty", in *IEEE Industry Applications Society Annual Meeting (IAS)*, 1991, pp. 1061-1066.
- [10] R. T. Bascopé and I. Barbi, "A Double ZVS-PWM Active-Clamping Forward Converter", in *IEEE Applied Power Electronic Conference and Exposition (APEC)*, 1999, pp. 596-601.
- [11] R. T. Bascopé and I. Barbi, "A Double ZVS-PWM Active-Clamping Forward Converter: Analysis, Design, and Experimentation", in *IEEE transactions on Power Electronics*, Vol.16, N°6, November 2001, pp. 745-751.